Alpha heating of indirect-drive layered implosions on the National Ignition Facility

K. L. Baker,[1,*] S. MacLaren,[1] O. Jones,[1] B. K. Spears,[1] P. K. Patel,[1] R. Nora,[1] L. Divol,[1] O. L. Landen,[1] G. J. Anderson,[1] J. Gaffney,[1] M. Kruse,[1] O. A. Hurricane,[1] D. A. Callahan,[1] A. R. Christopherson,[1] J. Salmonson,[1] E. P. Hartouni,[1] T. Döppner,[1] E. Dewald,[1] R. Tommasini,[1] C. A. Thomas,[2] C. Weber,[1] D. Clark,[1] D. T. Casey,[1] M. Hohenberger,[1] S. Khan,[1] T. Woods,[1] J. L. Milovich,[1] R. L. Berger,[1] D. Strozzi,[1] A. Kritcher,[1] B. Bachmann,[1] R. Benedetti,[1] R. Bionta,[1] P. M. Celliers,[1] D. Fittinghoff,[1] R. Hatarik,[1] N. Izumi,[1] M. Gatu Johnson,[3] G. Kyrala,[4] T. Ma,[1] K. Meaney,[4] M. Millot,[1] S. R. Nagel,[1] A. Pak,[1] P. L. Volegov,[4] C. Yeamans,[1] and C. Wilde[4]

[1]*Lawrence Livermore National Laboratory, Livermore, California 94550, USA*

[2]*Laboratory for Laser Energetics, University of Rochester, Rochester, New York 14623, USA*

[3]*Massachusetts Institute of Technology Plasma Science and Fusion Center, Cambridge, Massachusetts 02139, USA*

[4]*Los Alamos National Laboratory, Los Alamos, New Mexico 87545, USA*

(Received 28 May 2021; revised 7 August 2022; accepted 30 November 2022; published 9 January 2023)

In order to understand how close current layered implosions in indirect-drive inertial confinement fusion are to ignition, it is necessary to measure the level of alpha heating present. To this end, pairs of experiments were performed that consisted of a low-yield tritium–hydrogen–deuterium (THD) layered implosion and a high-yield deuterium–tritium (DT) layered implosion to validate experimentally current simulation-based methods of determining yield amplification. The THD capsules were designed to reduce simultaneously DT neutron yield (alpha heating) and maintain hydrodynamic similarity with the higher yield DT capsules. The ratio of the yields measured in these experiments then allowed the alpha heating level of the DT layered implosions to be determined. The level of alpha heating inferred is consistent with fits to simulations expressed in terms of experimentally measurable quantities and enables us to infer the level of alpha heating in recent high-performing implosions.

DOI: 10.1103/PhysRevE.107.015202

In an inertially confined fusion (ICF) implosion with a deuterium–tritium (DT) fuel layer, each fusion reaction of deuterium and tritium ions generates a 14.1-MeV neutron and 3.5 MeV alpha particle [1]. The areal density (ρR) required to stop the fusion neutron ($>5\,\mathrm{g/cm^2}$) is generally far above what is present in an ICF implosion [1]. As such, the majority of neutrons leave the implosion without interacting with the hotspot or the ice layer surrounding the hotspot. The stopping ρR for an alpha particle, however, is only $\sim$0.1 to $0.2\,\mathrm{g/cm^2}$ at an ion temperature, T_{ion}, of 4 keV, which is characteristic of the hotspot ρR and T_{ion} conditions achieved in many ICF implosions on the National Ignition Facility (NIF). Each of the alpha particles stopped within the hotspot deposit their 3.5 MeV of energy, increasing the hotspot T_{ion} and, subsequently, the reactivity rate. The ρR required to stop alpha particles increases with electron temperature (alpha-electron collisions are primarily responsible for stopping) such that alpha's not stopped in the hotspot are stopped in the cold DT fuel surrounding the hotspot, where ρR values are $\sim$0.4 to $1\,\mathrm{g/cm^2}$. The alpha particles stopped in the cold fuel heat and ablate the fuel into the hotspot, increasing the hotspot mass (M_{hs}) and the hotspot ρR, enabling more of the subsequent alpha particles to be stopped within the hotspot. An ignited plasma is one where the fusion heating power is high enough to overcome all of the physical processes that cool the fusion plasma. This creates a positive thermodynamic feedback loop with rapidly increasing temperature.

The radiation hydrodynamics code Hydra was used to perform a series of hydroscaled simulations covering a range of yield amplifications, Y_{amp}, from $\sim$1 to greater than 40 [2]. The capsule-only simulations perfectly hydroscaled the implosion at the time of peak kinetic energy, the start of the deceleration phase. The radiation temperature drive was linearly scaled in time by the scale factor S and the capsule dimensions were scaled by the scale factor S. This produced the same adiabat, implosion velocity etc. between the hydroscaled implosions. As the scale is increased, ρR also increases, which increases the self-heating and the yield amplification. These simulations were based on the BigFoot platform, as were the experiments described later, because at the time it had achieved the highest Y_{amp} levels on the NIF [3–8]. This level of performance has been surpassed in recent high-yield shots, but the Bigfoot data set allows validation of the technique described later. Determining the degree that alpha heating contributes to the yield is straightforward in simulations as alpha heating can be turned off. The Y_{amp} from these simulations can be fit by simulation parameters with experimental counterparts that can be directly measured. Fits based on these simulations for the ignition threshold factor, ITFXmod, and the yield amplification, $Y_{\mathrm{amp-ITFXmod}}$, are given in Eqs. (1) and (2):

$$\mathrm{ITFXmod} \sim (19.7 * \mathrm{DSR})^2 \times [0.24 \times (4 f_D f_T) \times Y_{13-15}/(M_{\mathrm{fuel}})] \quad (1)$$

*baker7@llnl.gov

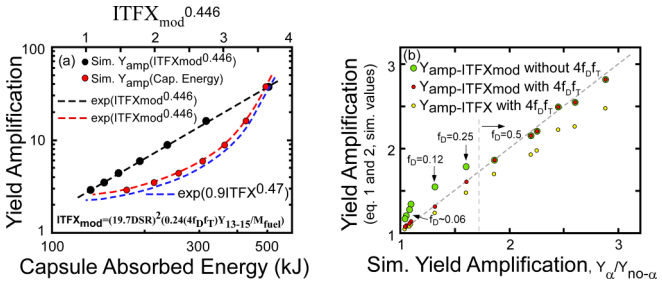

FIG. 1. (a) Simulated $Y_{\rm amp}$ as a function of the capsule-absorbed energy (red circles) and the modified ignition threshold factor (black circles), ITFXmod. The fits to simulations expressed in terms of experimentally measurable quantities [Eqs. (1) and (2)], along with the simulated DSR, primary yield, and ice mass are plotted as the dashed black and red lines. Fit using the conventional $Y_{\rm amp-ITFX}$ is plotted as a dashed blue line. (b) Motivates the inclusion of the factor $4f_Df_T$ in Eq. (1). In a DT implosion, this factor reduces to one, but for THD implosions, this factor was introduced to enable Eqs. (1) and (2) to provide an improved fit (red circles) versus not including $4f_Df_T$ in Eq. (1) (green circles) for those cases where the deuterium fraction was less than 0.5. Also shown is the conventional $Y_{\rm amp-ITFX}$, with an inclusion of $4f_Df_T$ (yellow circles).

and

$$Y_{\rm amp-ITFXmod} \sim \exp({\rm ITFXmod}^{0.446}), \tag{2}$$

where DSR is the down-scattered ratio (the ratio of the neutron yield in the neutron kinetic energy range from 10 to 12 MeV to the 13- to 15-MeV range), f_D is the deuterium number fraction in the hotspot, f_T is the tritium number fraction in the hotspot, Y_{13-15} is the primary neutron yield/10^{16} and $M_{\rm fuel}$ is the initial mass of the ice layer in milligrams. These fits are very similar to the equations determined for the $Y_{\rm amp}$ in direct-drive implosions [9] and in indirect-drive implosions [10]. The modified yield amplification fit in Eqs. (1) and (2), $Y_{\rm amp-ITFXmod} \sim \exp\{7.56 \times {\rm DSR}^{0.9}[(4f_Df_T)Y_{13-15}/M_{\rm fuel}]^{0.45}\}$, differs slightly from the conventional yield amplification, $Y_{\rm amp-ITFX} \sim \exp[8.67 \times {\rm DSR}^{0.99}(Y_{13-15}/M_{\rm fuel})^{0.47}]$ [10], calculated from the ignition threshold factor, ITFX. The simulated $Y_{\rm amp}$ as a function of capsule absorbed energy, red circles, and ITFXmod$^{1.3}$, black circles, are shown in Fig. 1(a), along with the dashed-line fits calculated from Eqs. (1) and (2) (red and black), and the conventional ITFX (blue) using simulated observables. These simulations added preheat energy to the DT ice (0.75 MJ/g) a few hundred picoseconds before the time of peak implosion velocity, which enabled them to match the experimental observables for this platform. This added ~70 J to a 45-μm-thick DT ice layer and changed the adiabat from the design of 4.0 to approximately 5.9. A separate set of Hydra simulations encompassing the experiments performed in this campaign were also conducted to test the scaling of Eqs. (1) and (2) on tritium–hydrogen–deuterium (THD) implosions, where the fraction of deuterium ions in the ice layer was less than 50%. These simulation results are shown in Fig. 1(b), where the simulated $Y_{\rm amp}$ for each implosion is represented on the x-axis and the fit using Eqs. (1) and (2) with simulated DSR, primary yield, and ice mass is represented on the y-axis. These simulations led to the incorporation of the term $4f_Tf_D$ in Eq. (1). With this term included (red circles), Eqs. (1) and (2) provided good fits to both the DT- and THD-simulated $Y_{\rm amp}$. When this term was removed from Eq. (1) (green circles), the fit overestimated the $Y_{\rm amp}$ for THD implosions with $f_D < 0.5$.

The level of alpha heating in DT layered implosions can be determined by comparing the yield of a hydrodynamically similar implosion with diluted fuel to that of a 50/50 DT layered implosion. The diluted fuel consists of specific ratios of tritium, hydrogen, and deuterium ions to conserve the layer mass, usually with the deuterium fraction being very small (around 5%) to limit the yield and the $Y_{\rm amp}$ [11,12] Specifically, the fraction of hydrogen atoms, n_H, and tritium atoms, n_T, in terms of the number of deuterium atoms, n_D, is given by $n_H = 0.25$–$0.5 \times n_D$ and $n_T = 0.75$–$0.5 \times n_D$ [11,12]. The $Y_{\rm amp}$ of the DT experiment can then be determined from the relationship

$$Y_{\rm amp} \equiv \frac{Y_{\rm DT}}{Y_{{\rm DT}\alpha-{\rm off}}} = \frac{Y_{\rm DT}}{Y_{\rm THD}} \frac{Y_{\rm THD}}{Y_{{\rm THD}\alpha-{\rm off}}} \frac{Y_{{\rm THD}\alpha-{\rm off}}}{Y_{{\rm DT}\alpha-{\rm off}}}, \tag{3}$$

where $Y_{\rm DT}$ and $Y_{\rm THD}$ are the yields measured in the separate DT and THD fuel experiments using nominally identical targets and laser drives, and $Y_{{\rm DT}\alpha-{\rm off}}$ is the DT yield if alpha particles did not deposit their energy in the hotspot or ice layer. The ratio $Y_{\rm THD}/Y_{{\rm THD}\alpha-{\rm off}}$ is slightly above 1 (1.04 to 1.14) due to a reduced, but nonzero, alpha heating contribution to its yield for the THD implosions described herein. This is estimated from simulations or Eqs. (1) and (2) and varies primarily due to the fuel composition in the THD implosion. The ratio of $Y_{{\rm THD}\alpha-{\rm off}}/Y_{{\rm DT}\alpha-{\rm off}}$ is given by the ratios of products of reactant fractions multiplied by factors correcting for hydrodynamic similarity deviations:

$$\frac{Y_{{\rm THD}\alpha-{\rm off}}}{Y_{{\rm DT}\alpha-{\rm off}}} \approx \frac{f_{D_{\rm THD}} f_{T_{\rm THD}}}{f_{D_{\rm DT}} f_{T_{\rm DT}}} \frac{1}{\beta} \left[\frac{1-(v_{{\rm hs}_{\rm THD}}/v_{{\rm imp}_{\rm THD}})^2}{1-(v_{{\rm hs}_{\rm DT}}/v_{{\rm imp}_{\rm DT}})^2} \right]^{3.6} \times \left(\frac{v_{{\rm imp}_{\rm THD}}}{v_{{\rm imp}_{\rm DT}}} \right)^{6.2}. \tag{4}$$

A value of $\beta \sim 1.3$ represents the average value of β versus ITFX for a range of simulations required to correct $Y_{{\rm THD}\alpha-{\rm off}}/Y_{{\rm DT}\alpha-{\rm off}}$ for deviations from hydrodynamic similarity between the THD and no-alpha heating DT layered implosions. These deviations are due to adiabat (compression) and THD concentrations at the place of peak weighted neutron burn, as seen in Fig. 6(a) in Ref. [13]. For this work, we also corrected the 1D yield for the differences in the residual mode one hotspot velocity observed between the DT and THD implosions using the analytic expression $Y\,\alpha[1-(v_{\rm hs}/v_{\rm imp})^2]^{3.6}$, where $v_{\rm hs}$ is the velocity of the hotspot and $v_{\rm imp}$ is the peak implosion velocity of the capsule [14–16]. This led to corrections in $Y_{\rm amp}$ of up to ±16%. The yield is also corrected for differences in the implosion velocities of the DT and THD implosions, using the analytic expression $Y\alpha v_{\rm imp}^{6.2}$ [14]. The difference in implosion velocity between the DT and THD pairs, however, were all less than ~2%, which is less than the absolute precision of the velocity from the simulation (±3.5%).

These experiments were conducted using the BigFoot platform and they were carried out with two different hohlraum and capsule sizes [3–8]. The experiments used high-density carbon (HDC) capsules with an inner-capsule radius of

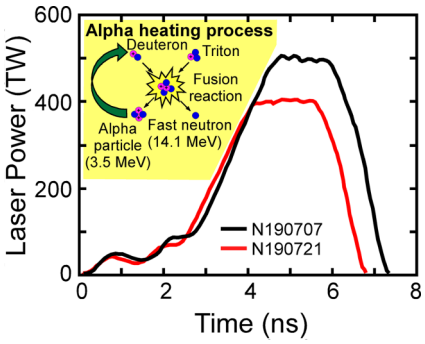

FIG. 2. Laser power as a function of time for the larger scale N190707 layered implosion (black line) and for the smaller scale N190721 implosion (red line). (Insert) A schematic of the alpha heating process in which alpha heating of the plasma increases the temperature and reaction rate of the fusion process.

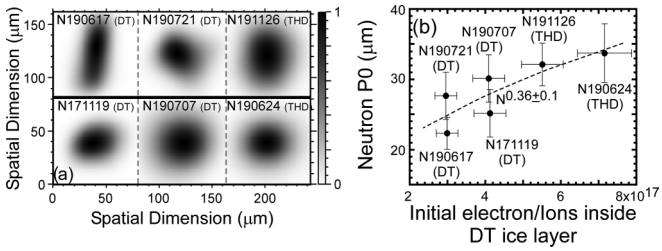

FIG. 3. (a) The primary neutron images for the six implosions used in the alpha heating campaign. The smaller scale DT–THD pairs of neutron images are shown at the top of the figure, with the two DTs on the left-hand side. The larger scale DT–THD pairs of neutron images are shown at the bottom of the figure, with the two DTs again on the left-hand side. (b) The initial electron density inside the ablator as a function of the final hotspot radius, *P*0.

950 (844) μm for the larger scale (smaller scale), and the capsule thickness was 72 (68.3) μm for the larger scale (smaller scale). The capsule walls were comprised of three layers: an outer, ∼44.5 (40.4)-μm-thick pure HDC layer, followed by an ∼21.4 (21.9)-μm-thick tungsten-doped layer with average dopant levels of 0.24% (0.32%) atomic fraction, and an innermost, undoped HDC layer of 6.3 (6) μm for the larger scale (smaller scale). The fusion fuel added to the inside of the capsules, THD or DT, had a layer thickness of ∼45 (40) μm for the larger scale (smaller scale). These capsules were placed in the center of a gold hohlraum of 11.3 (10.13) mm in length and 6.0 (5.4) mm in diameter with laser entrance holes at either end of the hohlraum, with a diameter of 3.9 (3.45) mm for the larger scale (smaller scale). The hohlraums in both cases were filled with low-density 4He gas at 0.3 mg/cm^3 to tamp the expansion of hohlraum wall and ablator material, provide heat conduction to the hohlraum walls, and minimize the laser–plasma instabilities inside the hohlraum. The pulse shapes used for the larger (black) and smaller (red) scale experiments are shown in Fig. 2. Both the DT layered implosion and the THD layered implosion performed at each scale used the same laser pulse shape.

When determining the Y_{amp} present in the experiments, the relative hotspot mass originating from the vapor and from the ice must be determined so as to calculate the effective hotspot concentrations used in Eqs. (1) and (3). The hotspot mass can be expressed as $M_{\mathrm{hs}} = \rho V_{\mathrm{hs}}$ and was calculated from the experimental measurables using the methods in Ref. [17] and assuming the hotspot radius was 1.28× the 17% contour of the neutron image. This choice of the hotspot radius enabled the simple homogeneous model to agree more closely with the hotspot mass inferred from three-dimensional reconstructions of the hotspot neutron image.

To estimate the hydrogen, deuterium, and tritium fractions in the hotspot, the initial ratios of hydrogen isotopes in the solid fuel layer and in the saturated vapor interior to that layer were calculated. The composition of the majority of the solid ice is the same as the initial reservoir gas mixture used to fill the capsule. Following a layering time (∼17 hours), the solid reaches an equilibrium with the six diatomic molecular hydrogen species: H_2, D_2, T_2, HD, HT and DT [18]. The composition of the saturated vapor in the initial central gas region is in solid/vapor equilibrium with the solid layer and is determined by this species' equilibrium. In the 30 seconds prior to a NIF shot, the capsule is rapidly cooled by 0.8 K, a mini-quench, which sets the vapor concentrations in the center of the ablator at shot time. The initial vapor mass concentrations calculated this way along with the ice concentrations are listed in the second column of Table I. Given the final hotspot mass and the initial vapor mass concentrations inside the fuel, the effective THD concentration in the hotspot were determined and are also listed in the second column of Table I within the square brackets. Given these final hotspot concentrations, the Y_{amp} can be calculated using Eqs. (3) and (4) and compared with the fits to simulations expressed in terms of experimentally measurable quantities expressed in Eqs. (1) and (2). In the DT layered implosions with a ∼50/50 deuterium/tritium reservoir, this also leads to a slightly higher deuterium concentration in the hotspot than the optimal 50/50.

One of the deviations from hydrodynamic similarity between the DT and THD experimental pairs, represented by the β term in Eq. (4), can be seen in the neutron hotspot images in Fig. 3(a) [19]. The initial saturated vapor concentrations inside the ice layer for each of the implosions is shown in Table I (column 2, in parentheses) along with the ice composition. This vapor is hydrogen/deuterium rich relative to the ice layer due to the difference in vapor pressure of the deuterium, tritium and hydrogen [20]. This leads to a higher initial electron density for the vapor inside the ice layer for the THD implosions, which have a majority of hydrogen in the vapor in comparison to deuterium for the DT implosions. This higher initial number of electrons in the THD implosions is correlated to the final hotspot radius, as shown in Fig. 3(b). In the THD implosion simulations, the peak of the burn was located some tens of micrometers away from the center due to the radial distribution of gas species, which also resulted in a larger hotspot than the corresponding DT implosion. In future experiments, the initial electron density can be reduced in the THD layered implosions by performing a larger quench (up to 1.5 K) than the DT implosion, reducing the β term in Eq. (4).

When the terms in Eqs. (3) and (4) are calculated, the experimental yield amplification can be determined as shown in Fig. 4. Fig. 4(a) shows the primary yield from each of the DT and THD implosions as blue bars. To

TABLE I. Summary of the two pairs of DT/THD experiments for which Y_{amp} has been determined experimentally.

Shot No.	Ice (gas) [hotspot] composition THD (%)	M_{hs} (μg) [f_T/f_D]	M_{vap} (μg) [frac]	Total yield (10^{14}) [sim]	v_{hs}/v_{imp}	v_{imp} (km/s)	Y_{THD} $Y_{DT\alpha-off}$	Y_{THD} $Y_{DT\alpha-off}$ corr.	Y_{amp} Eqs. (3) and (4) $M1$ corr.	Y_{amp} Eqs. (1) and (2) [sim]
N171119 DT 6 × 11.3	49.63:0.19:50.18 (33.85:0.67:61.6) [46.4:0.29:52.5]	7.7 [0.88]	1.56 [0.2]	112 [114]	0.12	411	0.126	0.089	2.6	2.4 [2.25]
N190707 DT 6 × 11.3	49.09/0.18/50.72 (32.75:0.66:61.3) [46.3:0.26:52.6]	8.9 [0.88]	1.56 [0.17]	69.1 [73.4]	0.20	426	0.126	0.113	1.7	1.9 [1.86]
N190624 THD 6 × 11.3	71.22/23.06/5.72 (18.9:73.3:3.1) [59.6:34.2:5.14]	7.35 [11.3]	1.63 [0.22]	3.86 [3.62]	0.22	420	N/A	N/A		1.1 [1.05]
N190617 DT 5.4 × 10.13	49.41/0.18/50.41 (32.8:0.65:60.85) [46.7:0.26:52.1]	6.8 [0.90]	1.1 [0.16]	74.5 [76.8]	0.28	432	0.157	0.173	2.1	2.2 [2.2]
N190721 DT 5.4 × 10.13	50.48/0.18/49.34 (34.4:0.65:60.4) [48.7:0.23:50.5]	*9.87* [0.96]	1.1 [0.12]	107 [112]	0.13	428	0.155	0.119	2.4	2.5 [2.6]
N191126 THD 5.4 × 10.13	71.47:21.87:6.67 (15.6:81.3:3.1) [62.6:31.3:6.1]	*7.85* [10.27]	1.24 [0.15]	5.38 [5.38]	0.20	433	N/A	N/A		1.14 [1.09]

isolate the yield dependence on reactant concentrations, the green bars represent the yield of the THD divided by the right-hand side of Eq. (4) (without the $M1$ and v_{imp} corrections or $Y_{THD}\beta f_{D_{DT}} f_{T_{DT}}/f_{D_{THD}} f_{T_{THD}}$, and the red bars represent the green bars divided by the small Y_{amp} of the THD pair or $Y_{THD\alpha-off}\beta f_{D_{DT}} f_{T_{DT}}/f_{D_{THD}} f_{T_{THD}}$. The Y_{amp}, without $M1$ or v_{imp} corrections, is then simply the ratio of the DT primary yield (blue bar) to the red bar or $Y_{DT\alpha} f_{D_{THD}} f_{T_{THD}}/(Y_{THD\alpha-off}\beta f_{D_{DT}} f_{T_{DT}})$. Fig. 4(b) represents the

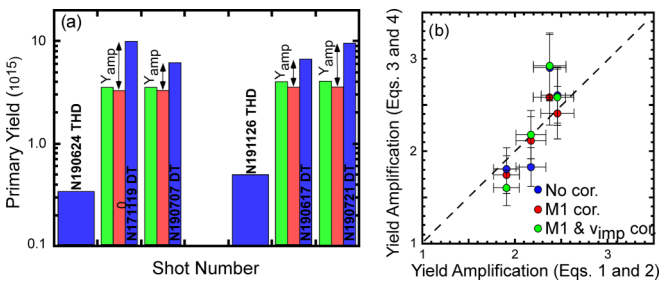

FIG. 4. (a) The primary yield and Y_{amp} from each of the DT and THD implosions. The blue bar represents the primary yield, the green bar represents the yield of the THD divided by Eq. (4) (without $M1$ and E_L corrections), and the red bar represents the green bar divided by the calculated Y_{amp} of the THD. (b) Y_{amp} as determined from the measurements in the experiments, as given by Eqs. (3) and (4), as a function of Y_{amp} using the down-scattered ratio, the initial DT mass, and the primary yield, as given by Eqs. (1) and (2). Blue circles represent no $M1$ or laser power P_L corrections, red circles represent an $M1$ correction between the THD implosion and the no-alpha DT implosion, and the green circles represent both an $M1$ and a P_L correction between the THD implosion and the no-alpha DT implosion.

Y_{amp} as determined from the measurements in the experiments, as given by Eqs. (3) and (4), as a function of the Y_{amp} using the empirical fit of the DSR, the initial DT mass, and the primary yield, as given by Eqs. (1) and (2). In Fig. 4(b), the blue circles include the Eq. (4) approximation without $M1$ or v_{imp} corrections. The red circles also include the Eq. (4) approximation with $M1$ but without v_{imp} corrections, and the green circles include all of the corrections listed in Eq. (4). As can be observed in Fig. 4(b) and in Table I, the Y_{amp} determined from the DT/THD pairs is within 20% of the Y_{amp} fit to simulations [Eqs. (1) and (2)] that has previously been applied to DT shots on the NIF. Ensemble simulations were performed on the implosions and closely matched the experimental yield, within 7%, and Y_{amp} inferred using Eqs. (1) and (2), within 6% with the $M1$ correction. Both the yield (column 5) and Y_{amp} (column 11) from the simulations are shown in Table I within the square brackets.

The ignition threshold factor can also be used to formulate a generalized Lawson criteria (GLC) for ignition, which includes alpha heating and uses only the directly measured quantities of DSR, primary neutron yield, and the initial ice mass. The previously defined GLC $= (P_{stag}/420)(E_{hs}/30)^{0.5}$ can be used along with the database of NIF layered implosions to determine the power scaling of ITFXmod resulting in a linear relationship between the two GLC definitions [21]. The stagnation pressure, P_{stag}, and hotspot energy, E_{hs}, used in this GLC are defined in Ref. [21] in Eqs. (17) and (14). Fig. 5 then shows that a definition of

$$\mathrm{GLC(ITFXmod)} = 0.27(\mathrm{ITFXmod})^{0.6} \tag{5}$$

provides a linear relationship between the two generalized Lawson criteria, GLC(ITFXmod) as defined by Eq. (5) and the previously defined $GLC(P_{stag}, E_{hs}) = (P_{stag}/420)(E_{hs}/30)^{0.5}$,

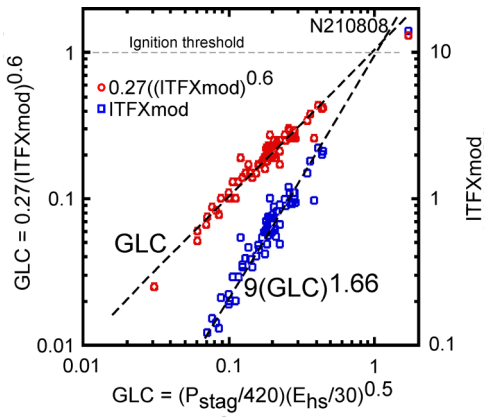

FIG. 5. Linearity of the generalized Lawson criterion using the GLC(ITFXmod) = $0.27(\text{ITFXmod})^{0.6}$ defined in Eq. (2) plotted against the GLC(P_{stag}, E_{hs}) = $(P_{\text{stag}}/420)(E_{\text{hs}}/30)^{0.5}$. Both GLCs are calculated using the neutron metrics from the existing database of experimental DT layered implosions on the NIF. Also plotted is the ITFXmod as defined in Eq. (1).

both of which include alpha heating. Fig. 5 also has plotted the ITFXmod for each of the experiments as a function of the GLC(P_{stag}, E_{hs}), and the fit to ITFXmod, ITFXmod = $9[\text{GLC}(P_{\text{stag}}, E_{\text{hs}})]^{1.66}$, implies a value of ITFXmod = 9 at the ignition threshold, GLC(P_{stag}, E_{hs}) = 1. At this value of ITFXmod, the yield amplification exceeds a value of ∼14.4. As seen in Fig. 5, the implosion N210808 exceeds the threshold for ignition, GLC = 1, as reported in Ref. [22].

A series of experiments using pairs of THD/DT layered implosions was conducted on the NIF to measure the level of alpha heating present in these implosions to understand how close they were to the burning plasma regime ($Y_{\text{amp}} \leqslant 3.5$) and to ignition ($Y_{\text{amp}} > 15$). These experiments allowed us to measure Y_{amp} experimentally with small corrections from simulations. We were also able to compare these measurements with fits to hydroscaled simulations of the BigFoot platform and confirm that Y_{amp} for these implosions were within ∼20% using these two methods. Over the Y_{amp} range studied in this campaign (1.7 to 2.9), we found good agreement between the experimentally inferred Y_{amp} and fits to simulation databases based on experimental observables, primary yield, DSR, and initial layer mass, thus using experiments and simulations to verify the consistency of the alpha heating models used to estimate Y_{amp}. Verification of Eqs. (1) and (2) with experiments enables us to look at more recent higher performing implosions and verify the levels of alpha heating present in those experiments. The DT implosions on the NIF were also used to define a generalized Lawson criteria, which includes alpha heating, based on the ignition threshold factor, ITFXmod, as given by Eq. (5). The recent high-performing shot N210808 with a DSR or 2.72%, an initial ice mass of 220 μg, and a primary yield of 4.3×10^{17}, is predicted by Eqs. (1) and (2) to have a yield amplification for that implosion at 24.8 ± 6.2, and the generalized Lawson criteria defined in Eq. (5) indicates that this implosion was past the ignition threshold of GLC = 1, as reported in Ref. [22].

ACKNOWLEDGMENTS

We wish to thank the NIF operations team. This paper was prepared by LLNL under Contract No. DEAC52-07NA27344. This document was prepared as an account of the work sponsored by an agency of the United States government. Neither the United States government nor Lawrence Livermore National Security, LLC, nor any of their employees, makes any warranty, expressed or implied, or assumes any legal liability or responsibility for the accuracy, completeness, or usefulness of any information, apparatus, product, or process disclosed, or represents that its use would not infringe privately owned rights. Reference herein to any specific commercial product, process, or service by trade name, trademark, manufacturer, or otherwise does not necessarily constitute or imply its endorsement, recommendation, or favoring by the United States government or Lawrence Livermore National Security, LLC. The views and opinions of the authors expressed herein do not necessarily state or reflect those of the United States government or Lawrence Livermore National Security, LLC, and shall not be used for advertising or product endorsement purposes.

[1] S. Atzeni and J. Meyer-ter-Vehn, *The Physics of Inertial Fusion* (Oxford Science Press, Oxford, 2004).

[2] M. M. Marinak, R. E. Tipton, O. L. Landen, T. J. Murphy, P. Amendt, S. W. Haan, S. P. Hatchett, C. J. Keane, R. McEachern, and R. Wallace, Three-dimensional simulations of Nova high growth factor capsule implosion experiments, Phys. Plasmas **3**, 2070 (1996).

[3] K. L. Baker *et al.*, Hotspot parameter scaling with velocity and yield for high adiabat layered implosions on the National Ignition Facility, Phys. Rev. E **102**, 023210 (2020).

[4] K. L. Baker *et al.*, High-Performance Indirect-Drive Cryogenic Implosions at High Adiabat on the National Ignition Facility, Phys. Rev. Lett. **121**, 135001 (2018).

[5] D. T. Casey *et al.*, The high velocity, high adiabat, Bigfoot campaign and tests of indirect-drive implosion scaling, Phys. Plasmas **25**, 056308 (2018).

[6] C. A. Thomas *et al.*, Deficiencies in compression and yield in x-ray driven implosions, Phys. Plasmas **27**, 112705 (2020).

[7] M. Hohenberger, D. T. Casey, C. A. Thomas, O. L. Landen, K. L. Baker, L. R. Benedetti, D. A. Callahan, O. A. Hurricane, N. Izumi, S. F. Khan, T. Ma, D. A. Mariscal, S. R. Nagel, A. Pak, and B. K. Spears, Maintaining low-mode symmetry control with extended pulse-shapes for lower-adiabat Bigfoot implosions on the National Ignition Facility, Phys. Plasmas **26**, 112707 (2019).

[8] R. Berger, C. A. Thomas, K. Baker, D. Casey, C. Goyon, J. Park, N. Lemos, S. Khan, M. Hohenberger, J. Milovich, D. Strozzi, M. Belyaev, T. Chapman, and A. B. Langdon, Stimulated backscatter of laser light from BigFoot hohlraums on the National Ignition Facility, Phys. Plasmas **26**, 012709 (2019).

[9] R. Betti, A. R. Christopherson, B. K. Spears, R. Nora, A. Bose, J. Howard, K. M. Woo, M. J. Edwards, and J. Sanz, Alpha

Heating and Burning Plasmas in Inertial Confinement Fusion, Phys. Rev. Lett. **114**, 255003 (2015).

[10] P. K. Patel *et al.*, Hotspot conditions achieved in inertial confinement fusion experiments on the National Ignition Facility, Phys. Plasmas **27**, 050901 (2020).

[11] M. J. Edwards *et al.*, The experimental plan for cryogenic layered target implosions on the National Ignition Facility: The inertial confinement approach to fusion, Phys. Plasmas **18**, 051003 (2011).

[12] B. K. Spears, S. Brandon, D. Clark, C. Cerjan, J. Edwards, O. Landen, J. Lindl, S. Haan, S. Hatchett, J. Salmonson, P. Springer, S. V. Weber, and D. Wilson, Prediction of ignition implosion performance using measurements of low-deuterium surrogates, J. Phys. Conf. Ser. **244**, 022014 (2010).

[13] J. Lindl, O. Landen, J. Edwards, E. Moses, and The NIC Team, Review of the National Ignition Campaign 2009–2012, Phys. Plasmas **21**, 020501 (2014).

[14] O. A. Hurricane, D. T. Casey, O. Landen, A. L. Kritcher, R. Nora, P. K. Patel, J. A. Gaffney, K. D. Humbird, J. E. Field, M. K. G. Kruse, J. L. Peterson, and B. K. Spears, An analytic asymmetric-piston model for the impact of mode-1 shell asymmetry on ICF implosions, Phys. Plasmas **27**, 062704 (2020).

[15] D. T. Casey *et al.*, Evidence of Three-Dimensional Asymmetries Seeded by HDC-Ablator Non-Uniformity in Experiments at the National Ignition Facility**,** Phys. Rev. Lett. **126**, 025002 (2021).

[16] J. Milovich, D. Casey, B. MacGowan, D. Clark, D. Mariscal, T. Ma, K. Baker, R. Bionta, K. Hahn, A. Moore, D. Schlossberg, E. Hartouni, S. Sepke, and O. Landen, Understanding asymmetries using integrated simulations of capsule implosions in low gas-fill hohlraums at the National Ignition Facility, Plasma Phys. Control. Fusion **63**, 025012 (2021).

[17] O. A. Hurricane *et al.*, Fuel gain exceeding unity in an inertially confined fusion implosion, Nature (London) **506**, 343 (2014).

[18] B. K. Spears (private communication).

[19] M. D. Wilke *et al.*, The National Ignition Facility Neutron Imaging System, Rev. Sci. Instrum. **79**, 10E529 (2008).

[20] P. C. Souers, *Hydrogen Properties for Fusion Energy* (University of California, Berkeley, 1986).

[21] J. D. Lindl, S. W. Haan, O. L. Landen, A. R. Christopherson, and R. Betti, Progress toward a self-consistent set of 1D ignition capsule metrics in ICF, Phys. Plasmas **25**, 122704 (2018).

[22] H. Abu-Shawareb *et al.*, Lawson Criterion for Ignition Exceeded in an Inertial Fusion Experiment, Phys. Rev. Lett. **129**, 075001 (2022).